Int. J. Multiphase Flow Vol. 7, pp. 63–81
Pergamon/Elsevier, 1981. Printed in Great Britain

0301-9322/81/0201-0063/$02.00/0

LOCAL CHARACTERISTICS OF UPWARD GAS–LIQUID FLOWS

V. E. NAKORYAKOV and O. N. KASHINSKY

Institute of Thermophysics, Siberian Branch of the U.S.S.R. Academy of Sciences, 630090, Novosibirsk, U.S.S.R.

and

A. P. BURDUKOV and V. P. ODNORAL

Special Designing Body "Energokhimmash", 630056, Novosibirsk, U.S.S.R.

(*Received* 15 *August* 1979; *in revised form* 3 *July* 1980)

Abstract—The results of two-phase flow structure measurements in an upward gas–liquid flow in a 86.4 mm i.d. tube by the electrochemical and conductivity techniques are presented. Measurements were made in bubble and slug flow regimes at liquid flow rates ranging from 0.2 to 2 m/s.

The flow instability and ambiguity in a bubble regime at low liquid velocities is shown to exist. Great discrepancy between measured wall shear stress values and those predicted by the Lockhart–Martinelli model are due to the nonuniform distribution of gas over the tube cross section. Measurements of intensity of wall shear stress and liquid velocity fluctuations in a two-phase flow are presented.

1. INTRODUCTION

An extensive application of two-phase flows in such fields of the modern technology as energetics, chemical technology, oil and gas transport places demands on the engineering methods of their prediction. The available classical methods of two-phase flow prediction are based on the measurements of global characteridtics (Lockhart & Martinelli 1949, Armand 1946). These methods are one-dimensional and utilize extremely simplified two-phase (homogeneous or annular) flow models. The development of modern two-dimensional methods similar to those applied in the hydrodynamics of single-phase flows, is constrained by insufficient experimental data on the internal flow structure, which can be obtained only from the measurements of local turbulent characteristics. The general flow structure is qualitatively described by separating various flow regimes. In a vertical tube the main regimes are bubble, slug and annular-disperse flows. However, the separation into flow regimes only roughly describes the main characteristics of two-phase flows. Knowledge is still lacking on the flow structure within the same regime and on the effect of different parameters (flow rates of different phases, liquid and gas physical properties, tube geometry) on it.

The study of local gas–liquid flow characteristics was started from the measurements of the local void fraction profiles (Neal & Bankoff 1963, Delhaye 1968) by the conductivity and hot-film techniques. Later on the distribution of the local void fraction was studied by the above methods and by the γ-ray and optical probe techniques (Kazin 1964, Galaup 1975). The application of a double electroconductivity probe permits determining the gas-phase velocity (Serizawa 1975, Galaup 1975). In the same studies the liquid phase velocity profiles and the RMS values of gas and liquid velocity fluctuations were measured.

To understand an overall flow structure and to elucidate the mechanism of turbulent transfer in two-phase flows, it is necessary to perform complex investigations involving measurements of the as high as possible number of hydrodynamic characteristics. At present only two this-type studies are known (Serizawa 1975, Herring & Davis 1976). Serizawa measured the local void fraction, velocity and intensity of liquid and gas velocity fluctuations in a 1800-mm long tube of 60 mm i.d. in a rather narrow (0.44–1.03 m/s) range of liquid velocities. Herring and Davis performed a detailed measurement of the profiles of void fraction and gas velocity in a

50.8-mm dia. tube in a wide range of liquid velocities from 1 to 6 m/s at variously organized two-phase flow on the inlet.

Likewise in single-phase flow, in two-phase turbulent flows of great interest should be the investigation of turbulent characteristics in the wall vicinity, since this region is characterized by the greatest liquid velocity gradients and the highest values of turbulent fluctuations. Greatly interesting are the local wall shear stress measurements giving the information on the profile slope near the wall and on its fluctuational values. Unfortunately, the wall boundary region has not been investigated.

In the present study along with the conductivity technique an electrochemical method was used (Mitchell & Hanratty 1966, Kutateladze *et al.* 1968) which permits us to measure the wall shear stress and liquid velocity as well as the intensity of fluctuations of their values.

2. EXPERIMENTAL TECHNIQUE

2.1 *Experimental set-up*

The experimental set-up is schematically shown in figure 1. Liquid was pumped through a flow loop by a centrifugal pump with the maximum flow rate of 50 m^3/h and pressure of 6 atm. The test section was a vertical 6.5 m long stainless-steel tube of 86.4 mm i.d. consisting of several sections. The two-phase flow was formed in a mixer installed on the test section input (figure 1b). Gas (air) was injected into flow through the side surface of porous 80 mm long and 40 mm dia. stainless-steel tube. At high velocity values the porous tube resistance did not

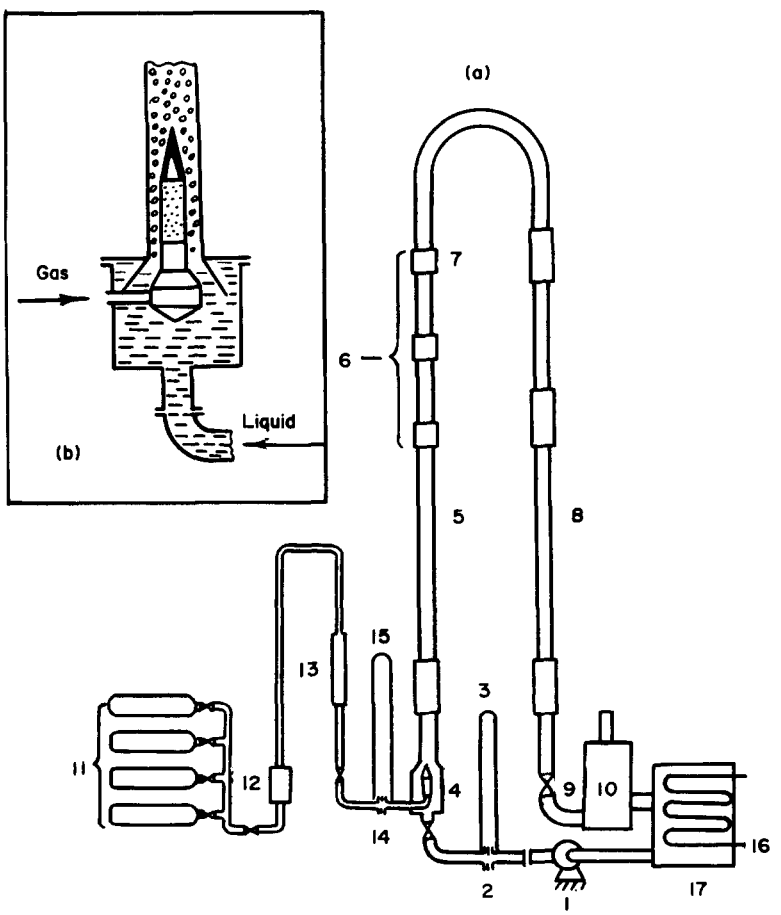

Figure 1. (a) Schematic diagram of experimental set-up: 1—pump, 2, 14—orifice meters, 3, 15—differential manometers, 4—mixer, 5—upward channel, 6—regions of visualization, 7—test section, 8—downward channel, 9—adjusting valve, 10—separator, 11—compressed air vessels, 12—filter, 13—heater, 16—heat exchanger, 17—storage tank. (b) Mixer.

permit the required gas flow rate to be obtained, and in this case gas was injected through a nozzle with a 20-mm orifice placed on the mixer axis. Liquid and gas flow rates were controlled with valves and measured by orifice meters. The test section pressure was kept constant by a valve on the section outlet. The temperature of the inlet liquid and gas was maintained at a constant level of 24 ± 0.5°C by automatic controllers. For visual flow picture observation the test section was supplied with several transparent plexiglass windows.

Two-phase flow characteristics were measured at a distance of 4.74 m from the gas input. The liquid velocity was varied from 0.22 to 2.05 m/s and the gas void fraction at the minimum and maximum liquid velocity was in the range of 0–80 and 0–50 per cent, respectively, which corresponded to bubble and slug flow regimes.

2.2 *Electrochemical method of hydrodynamic characteristics measurements*

The electrochemical method consists in measuring the rate of ion diffusion to the electrode where a rapid redox reaction occurs. Its schematic representation is given in figure 2. The test liquid is a solution of 0.01 N potassium ferri- and ferrocyanide in a background solution of 0.5 N of sodium hydroxide in distilled water. A shear stress probe (cathode) is the tip of a platinum plate installed flush with the tube wall. Anode is the set-up metallic section. When voltage is applied between anode and cathode the following reaction

$$Fe(CN)_6^{3-} + e^- \rightleftarrows Fe(CN)_6^{4-} \qquad [1]$$

occurs on the electrodes. As a result the concentration of $Fe(CN)_6^{3-}$ ions on the cathode is zero and due to the difference of concentrations between bulk and surface of the cathode the ferricyanide ions diffuse to it. The excess Na^+ and OH^- ions in the solution which are formed during the sodium hydroxide dissociation, create the high electroconductivity of the solution and eliminate the migration of active ions under the action of an electric field. The anode surface is by several thousands times larger than that of the cathode, therefore the anode current density is much lower and the processes taking place on the anode do not influence the current. Thus in the given conditions the circuit current is governed only by the diffusion of ferricyanide ions to the cathode. Due to the small cathode size and high Schmidt number (about 1500) the diffusion boundary layer formed on the cathode is embedded in a viscous sublayer so that within the diffusion layer the liquid velocity, u_1, is linearly dependent on the distance from wall, y

$$u_1 = \frac{\tau_w}{\mu} y \qquad [2]$$

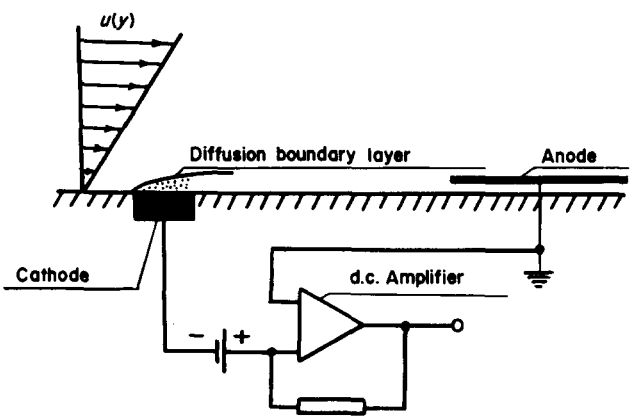

Figure 2. Schematic representation of electrochemical method of wall shear stress measurements.

where τ_w is the wall shear stress, μ is viscosity. The solution of the equation of diffusion boundary layer with the above velocity profiles provides the following correlation for the coefficient of mass transfer from the cathode, K (Reiss & Hanratty 1963)

$$\frac{KL}{D} = 0.807 \left(\frac{\tau_w L^2}{\mu D}\right)^{1/3}, \qquad [3]$$

where L is the longitudinal probe size, D is the diffusion coefficient of ferricyanide ions. The mass transfer coefficient is determined by the measured probe current, I, using the relation

$$K = \frac{I}{FSC_o} \qquad [4]$$

where S is the probe area, F is the Faraday number, C_o is the concentration of active ions. After measurement of the probe current, from [3] the wall shear stress can be determined

$$\tau_w = \frac{1.87\,\mu I^3}{F^3 C_o^3 D^2 L^2 h^3}, \qquad [5]$$

where h is the transverse probe size.

For liquid velocity measurements the cathode which is a velocity probe, is introduced into flow (figure 3). From the solution of the diffusion equation for the given probe configuration the relation between current and liquid velocity, u_1, near the probe is obtained

$$\frac{Kd}{D} = A_1 \left(\frac{u_1 k}{\nu}\right)^{1/2}, \qquad [6]$$

where d is the characteristic probe size and the A_1 coefficient is dependent on the electrode shape. In practice it is more convenient to represent the calibration relation for the given probe in the dimensional form as (Mizushina 1971).

$$I = A + B\sqrt{u_1}, \qquad [7]$$

where A and B are the calibration coefficients.

The case of measurements in flows with the time-dependent wall shear stress and velocity was considered theoretically by Bogolyubov *et al.* (1972) and by Bogolyubova & Smirnova (1977), respectively. The frequency response function $H(\omega_*)$ which is equal to the ratio between the fluctuations of electrochemical current and wall shear stress can be approximated

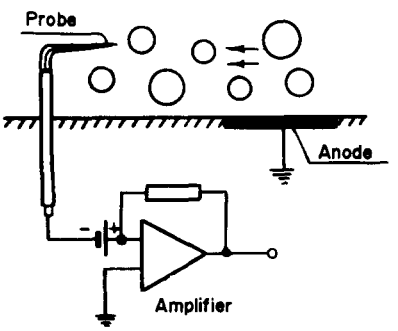

Figure 3. Liquid velocity measurements in two-phase flow by electrochemical method.

as

$$H(\omega_*)^2 = [(9 + 0.54\omega_*^2)^2 + (0.27\omega_*^3)^2]^{-1/2} \quad [7a]$$

where $\omega_* = \omega(L^2\mu^2/\tau_w^2 D)^{1/3}$ and ω are respectively the dimensionless and the angular frequencies. From [7a] it can easily be seen that at $\omega_* < 0.5H(\omega_*) \simeq H(0)$, so that for $\omega < \omega_q = 0.5(\tau_w^2 D/L^2\mu^2)^{1/3}$ the current would follow the instantaneous wall shear stress value. In this frequency range a quasi-steady approximation is valid. The ω_q value increases with decreasing the probe size. Thus, if $L = 0.02$ mm and $\tau_w = 1$ N/m^2, $\omega_q = 60$ s^{-1}. In these conditions the actual spectrum of wall shear stress fluctuations is disposed completely in the above frequency range. Therefore the frequency response function should be taken into account only for measurements of the high-frequency "tail" of the fluctuations spectrum.

Electrochemical wall shear stress probes were manufactured as follows. A platinum plate of the required cross section was welded into a glass tube which was then fitted in circumference and tightly inserted into a wall of the measuring unit. Then the probe face was sanded until it was placed flush with the tube wall. After sanding the probe was polished with an emery paper of gradually diminishing size. The face of the platinum plate being the cathode, was 0.1×1.5 and 0.02×0.2 mm^2 for the wall shear stress and its fluctuation measurements, respectively.

We have used velocity probes of the "blant nose" type, which is schematically represented in figure 4. The probe was made of a platinum 0.02-mm wire welded into a thin glass capillary of 0.05 mm o.d. The probe face was fitted, after which the probe was cemented in a stainless-steel holder of 3 mm o.d. The probe position in flow was controlled by a traversing 0.01 mm calibrated mechanism.

As a rule, in a two-phase flow there is a wall liquid film which is sufficient for the wall shear stress probe operation. Therefore as is shown by Kutateladze *et al.* (1968), the probe operation in two- and single-phase flows is essentially the same. At the same time the velocity probe operating in a two-phase flow, is alternately either in liquid or in gas. The current of the velocity probe is of the form shown in figure 5(a). Sharp drops correspond to the moments of probe

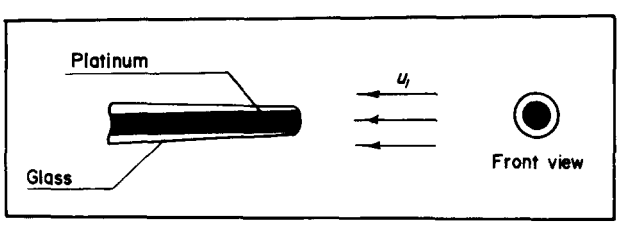

Figure 4. Electrochemical "blant nose" velocity probe.

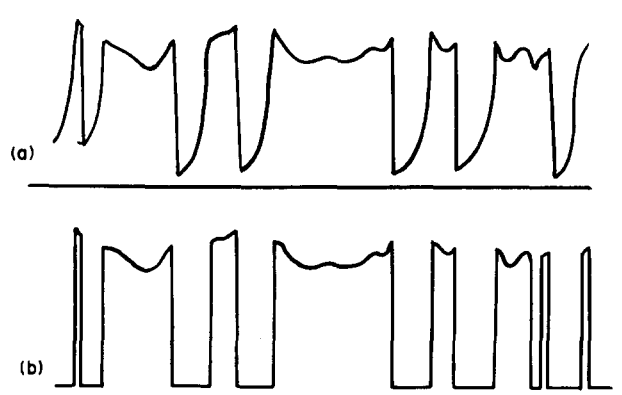

Figure 5. Signal of velocity probe in two-phase flow: (a) probe signal, (b) transformed signal.

residence in gas. Separate processing of the regions corresponding to liquid, provides mean and fluctuational liquid characteristics. Measuring the probe residence time in gas, one can obtain the local void fraction at a given point.

2.3 *Electronic equipment*

A schematic diagram of the electronic equipment is given in figure 6. The shear stress probe signal was fed to a d.c. amplifier with a probe feed circuit. The amplifier output voltage and intensity of fluctuations were measured by integrating and RMS (with an output integrator) voltmeters, respectively. The time of integration was 100 s.

A signal of the velocity probe was fed to an analog d.c. amplifier and its output signal was sent to a gate circuit. To simplify the detection of a gas phase, the velocity probe was connected in parallel with two low and high frequency electric circuits. The former was a usual circuit for the above single-phase electrochemical measurements (figure 3). The latter operating at a frequency of 100 kHz, was a usual circuit for an electroconductivity method (e.g. Herringe & Davis 1976). Thus the gas phase was detected by the well-elaborated conductivity method. The output signal of the high frequency circuit controlled the gate circuit, whose output and input voltages (figure 5(b)) were equal in magnitude at the moments corresponding to liquid and the output was zero at the moments corresponding to a gas phase. Since all measurements were performed in an upward gas–liquid flow, the bubbles velocity was higher than the local velocity of liquid at the same point. Hence the instantaneous velocity of liquid directly before and immediately after bubbles was higher than its time-averaged velocity which caused the appearance of signal peaks directly before and immediately after the bubbles passage. The gate output signal was fed to the computer ADC and converted to a digital form, after which it was processed. As a result the local void fraction, mean liquid velocities and RMS liquid velocity fluctuations were determined.

2.4 *Measurement accuracy*

To estimate the accuracy of liquid velocity measurements, the integrated local velocities were compared with the values obtained from the liquid flow rates. The discrepancy was within 3.5 per cent.

The only means to verify the accuracy of the local void fraction measurements was to compare the integrated void fractions with the values predicted by the Armand correlation [8]. The discrepancy was within 15 per cent except the regime with $U_l = 0.442$ m/s and $\beta = 0.265$, where the disbalance was 42 per cent. It is not surprising as at low U_l [8] can be wrong.

The accuracy of measuring the RMS values of wall shear stress and velocity was estimated as 10–15 per cent, if the ratio of the RMS and the mean values was no more than 0.5. In the

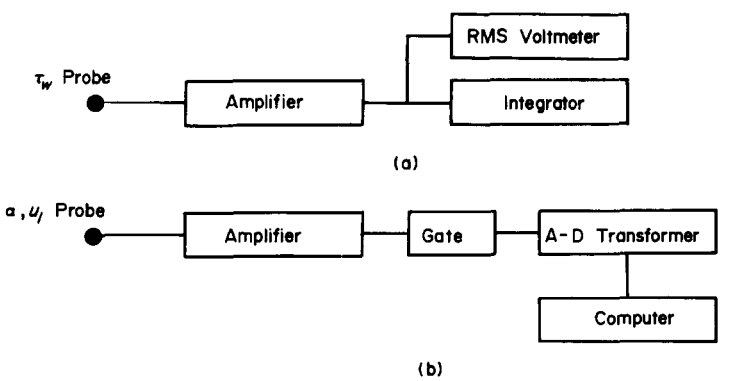

Figure 6. Block-diagram of electronic equipment. (a) wall shear stress measurements, (b) measurements of velocity and void fraction profiles.

case when the RMS/mean ~ 1, the possible errors might have been higher than 30 per cent, therefore these results should be considered actually as qualitative.

3. EXPERIMENTAL RESULTS

3.1 *Some properties of bubble flow*

The parameters of a two-phase flow were measured at liquid flow rates of 0.22, 0.44, 0.79, 1.03 and 2.05 m/s. The volumetric gas flow rate ratio $\beta = U_g/(U_g + U_l)$ varied from zero to the maximum value dependent on the liquid velocity and equal to 0.5–0.8. Under these conditions the flow was in bubble and slug regimes. The bubble regime studies show that its structure and parameters cannot be unambiguously determined by the given liquid and gas flow rates. The flow was slightly unsteady. In detail this phenomenon was studied at a liquid velocity of 0.79 m/s. The wall shear stress vs β is shown in figure 7(a). In this case the slug regime was observed at $\beta > 0.21$. However, the $\tau_w(\beta)$ dependence was not unambiguous. The bubble regime was as if there were two subregimes hereafter referred to as regimes A and B.

Let us describe one experiment. Successive measurements of τ_w values at constant U_l and variable β for a long time (about several hours) provide the picture shown by arrows in figure 7(a). Experimental points were first positioned on a lower curve (line I). In this case the bubble flow regime was realized. After reaching a certain maximum value on curve A, the wall shear stress began to decrease, gas bubbles increased and gas slugs were formed, whose size was commensurable with the tube diameter. But then during a short period of time at constant U_l and β the regime spontaneously returned to a pure bubble flow with a marked increase of the τ_w value. Then at further variation of β the points were positioned along the upper curve (line II). This direction of the flow process was not the only possible. Experimental points could primarily be positioned along line II with further transition to line I, then after a certain period of time a back transition could occur, etc. Multiple runs of the experiments show that both regimes A and B are sufficiently steady and can exist for a long time (from half an hour to several hours), while the transition between them occurs for 3–15 min and is random. To find some regularity the experiment was repeated several times with various direction of the β variation. In addition it has been verified whether the above effects were due to the operational mixer instability. For this purpose the experimental runs were repeated with the mixer porous tube prepurging for 1–1.5 h (the porous tube being placed above the liquid level) with

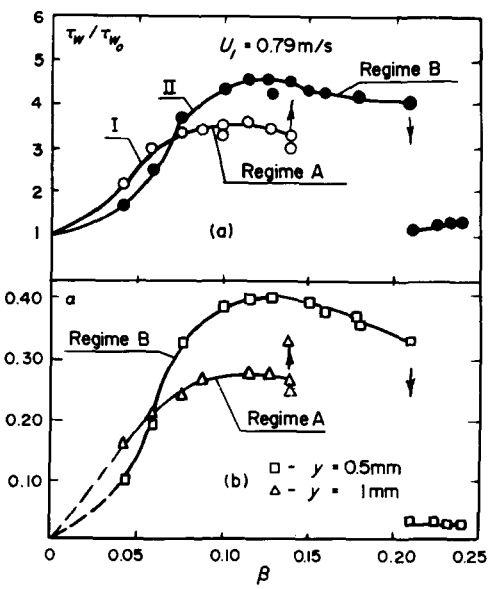

Figure 7. Wall shear stress, α, vs inlet gas flow rate.

subsequent liquid supply without turning off gas, as well as with primary liquid supply and subsequent gas introduction. Besides in several runs the gas supply was stopped for various periods of time. However the change of these factors exerted no influence on the flow behaviour.

To study the flow structure in A and B regimes in more detail the local void fraction was measured. Virtual values of the local void fraction α at two fixed points at a distance of 0.5 and 1 mm from wall are given in figure 7(b). α was measured simultaneously with the wall shear stress measurements. The bahaviour of α and τ_w at these points was qualitatively the same. The maximum values of α at all measured β values in regime A are observed at $y = 1$ mm from the channel wall. At A-to-B transition the maximum α values were observed even at $y = 0.5$ mm. In addition the α values in regime B significantly increase, e.g. at $\beta = 0.12$ in regimes A and B $\alpha = 0.28$ and 0.4, respectively. The transition to a slug regime was followed by a sharp decrease of α near the channel wall (at $\beta = 0.21$, $\alpha = 0.03$), i.e. gas departs from wall to tube center.

Profiles of the local void fraction $\alpha(r)$ in regimes A and B are shown in figure 8. It can be seen that in regime A the α value near wall is lower than in regime B at the same β. In the central part of the tube the situation is opposite.

Figure 9 represents flow photographs corresponding to the beginning of the A-to-B transition and to the fully completed transition to regime B. It can be seen that before the transition the flow structure is not purely bubble, at the centre of the tube large bubbles are formed. In addition a great scatter in the bubble sizes is observed. After the flow reconstruction into regime B the flow is purely bubble. The size of bubbles decreases, large bubbles at the tube center disappear, the flow structure becomes fairly uniform.

The above existence of two types of bubble regimes was observed at all liquid velocities except at 2.05 m/s. The qualitative flow behaviour was similar to that described at $U_l = 0.79$ m/s.

A flow pattern map with β and U_l axes is represented in figure 10. Symbols B and S correspond to pure bubble and pure slug flows, respectively. Symbol A refers to the region where ambiguous flow regimes are observed. The region of the bubble-to-fully developed slug flow transition is crosshatched. This region is characterized by a negative τ_w vs β slope (figures 11 and 12).

The existence of two different flow regimes at constant U_l and β is closely connected with different bubble size distributions. Regime B (figure 7) is characterized by relatively small bubble sizes of the order of 2–3 mm of magnitude. Their generation is due to the presence of sodium hydroxide and potassium ferro- and ferricyanide which leads to the surfactant proper-

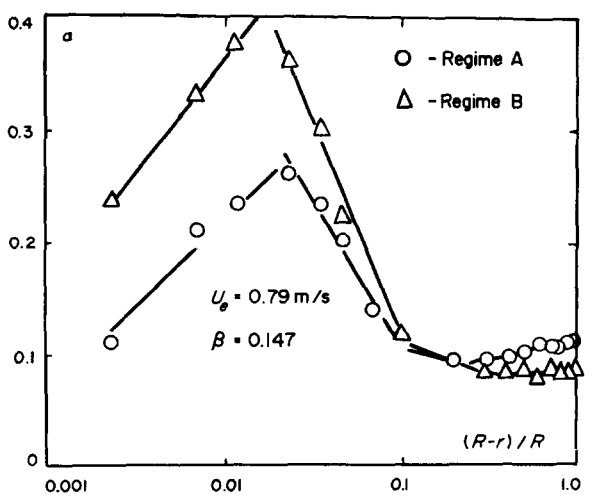

Figure 8. Local void fraction profiles.

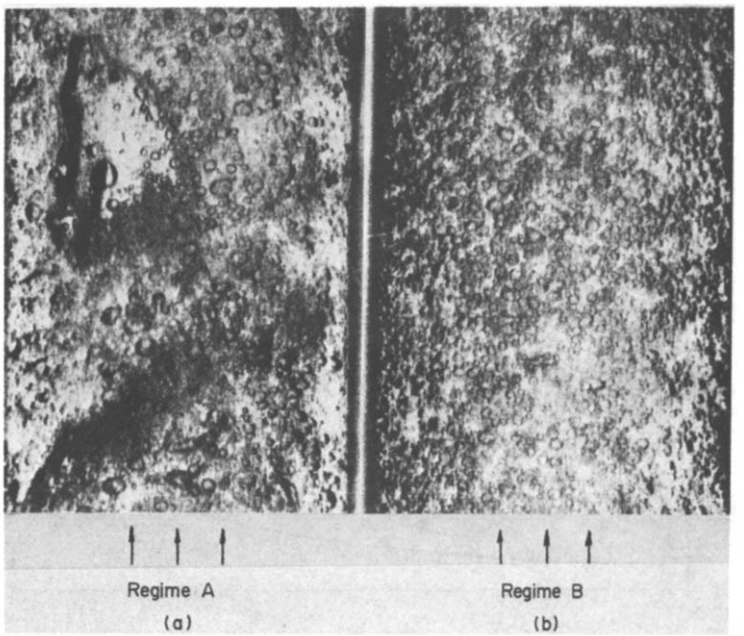

Figure 9. Flow photographs in channel: (a) beginning of A-to-B transition; (b) B regime (bubble flow).

ties of liquid also promoting bubbles fusion. It is likely that there should be some sort of competition between the potential energy of bubble surfaces intimately related to the bubble size distribution, and the kinetic energy of liquid turbulent fluctuations. Apparently, these two parts of the energy of a two-phase flow are of the same order of magnitude and there can exist energy exchange leading to the formation of different flow structures. This effect must be too fine and cannot be verified experimentally at present. It is likely that at given U_l and β only two states of flow corresponding to two weak minima of the curve of the total flow energy vs the bubble size distribution, are stable for a long time, namely regimes A and B. Certainly, all intermediate regimes can also exist but for a sufficiently short period of time of about several minutes. The A-to-B transitions are surely the results of small perturbations imposed on the inlet mean liquid and gas flow rates which cannot be eliminated.

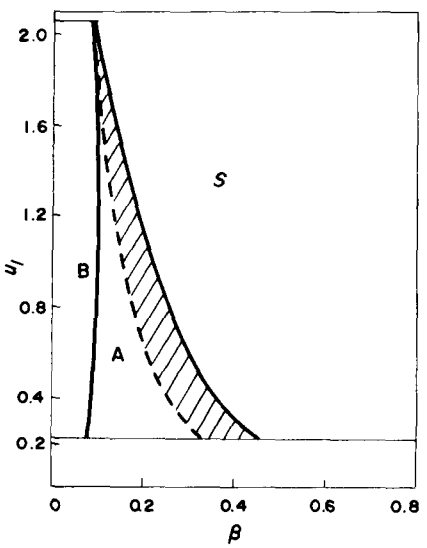

Figure 10. Flow pattern map.

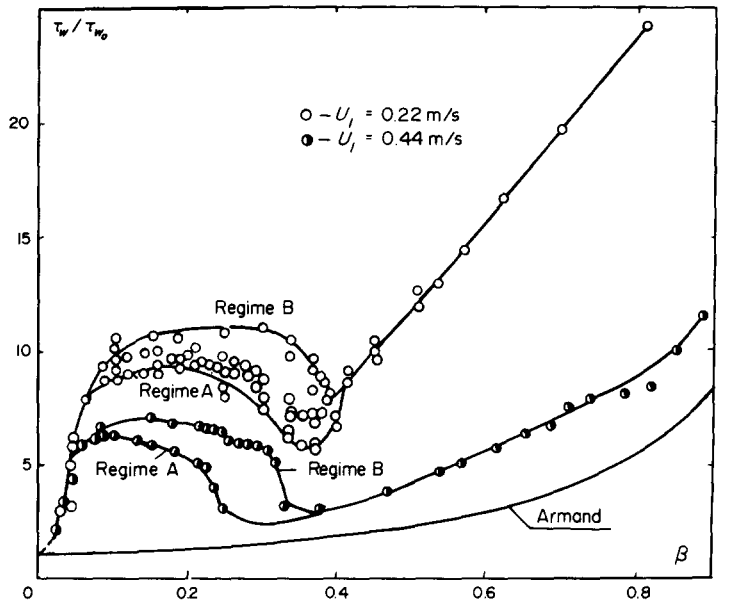

Figure 11. Wall shear stress vs gas flow rate.

With increasing U_l, the absolute values of the intensity of turbulent liquid velocity fluctuations rise. This causes "smearing" of the bubbles over the entire cross section and prevents their concentration near the tube walls and fusion, which ceases the flow ambiguity.

The strong effect of bubble size distribution on the properties of a gas–liquid flow at small liquid velocities was confirmed by direct experiments by Valukina *et al.* (1979), wherein the bubble size was controlled and maintained uniform.

3.2 *Wall shear stress*

Pressure drops due to the friction in a two-phase flow were measured in a great number of works (Lockhart & Martinelli 1949, Armand 1950, Govier *et al.* 1957). As a rule, measurements were performed in slug and annular-disperse regimes. The calculation methods elaborated on the basis of these calculations for low gas void fractions corresponding to a bubble flow regime, ensure small deviation of the friction losses in a two-phase flow from the respective value in a single-phase flow. Pressure drops due to the friction in a bubble flow regime were measured only in

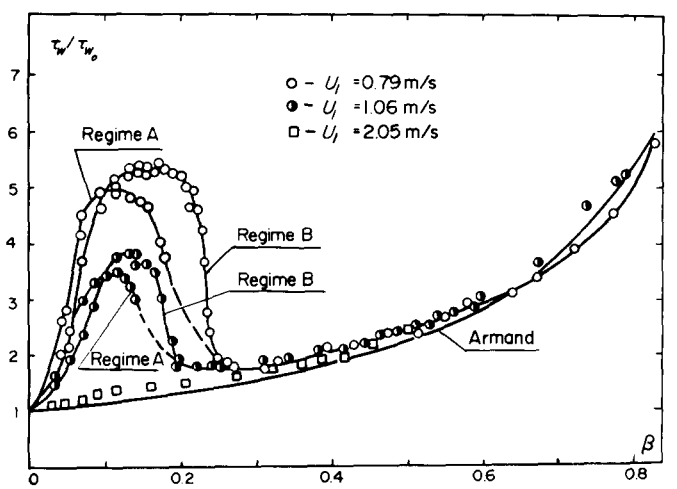

Figure 12. Wall shear stress vs gas flow rate.

a few studies (Aoki & Inoue 1965, Nakoryakov *et al.* 1973, Davis 1974, Kopalinsky & Bryant 1976).

Figures 11 and 12 present the results of our measurements in the coordinates $\tau_w/\tau_{w_o}(\beta)$, where τ_{w_o} is the wall shear stress in a single-phase flow at a liquid flow rate which is equal to that in a two-phase flow. Figures 11 and 12 represent both regimes A and B.

The calculation method (Armand 1950) gives the following relation between wall shear stress and gas void fraction

$$\tau_w/\tau_{w_o} = (1 - 0.833\beta)^{-1.53}. \qquad [8]$$

Other methods, e.g. Lockhart & Martinelli 1949, at low β provide relations close to [8]. All these relations ensure the monotonous τ_w/τ_{w_o} increase with β.

As is seen from the figures 11 and 12, the measured distributions of $\tau_w/\tau_{w_o}(\beta)$ in the general case significantly differ both quantitatively and qualitatively from [8]. First of all, the $\tau_w/\tau_{w_o}(\beta)$ is not monotonous. In the region of bubble flow regime τ_w/τ_{w_o} drastically increases even at small β. In the region of bubble-to-slug transition τ_w drops with β increase. The maximum τ_w/τ_{w_o} value in a bubble regime significantly depends on liquid velocity decreasing with its rise. The measured τ_w values are by several times higher than those calculated by [8]. In the region corresponding to the slug regime at $U_1 \geq 0.8$ m/s experimental points are in good agreement with the Armand formula. At lower liquid velocities there is a significant deviation from this formula which is typical for the flows with low Froude number, $\mathrm{Fr} < 2$ (Mamaev *et al.* 1969).

It is interesting to note that at the maximum liquid velocity, $U_1 = 2.05$ m/s, the measured τ_w values are in good agreement with [8] in all regimes. A similar result was experimentally obtained by Davis (1974) at high liquid flow rates. The behaviour of the friction coefficient at low velocities $U_1 < 1$ m/s is similar to that described by Aoki & Inoue (1965) and Nakoryakov *et al.* (1973). Unfortunately, these experiments were performed at significantly different tube diameters (28.8 and 15 mm, respectively), thus the direct quantitative comparison of the results is impossible.

The results of measuring the relative intensity of wall shear stress fluctuations, $\sqrt{(\overline{\tau_w'^2}/\overline{\tau_w})}$, are given in figure 13. As known (Laufer 1954, Hanratty 1966), in a tube single-phase flow this ratio is close to 0.3. In a bubble flow regime the intensity of wall shear stress fluctuations is slightly dependent on the void fraction and is somewhat higher than in a single-phase flow ($\sqrt{(\overline{\tau_w'^2}/\overline{\tau_w})} = 0.4 \div 0.6$). The dependence of this value on the liquid velocity is observed, i.e. with its increase the intensity of friction fluctuations approaches the value in a single-phase flow. In the region of slug flow regime a considerable rise in the wall shear stress fluctuations with increasing the gas flow rate is observed. In a fully-developed slug regime the $\sqrt{(\overline{\tau_w'^2}/\overline{\tau_w})}$ ratio can exceed unity which indicates a great difference in the instantaneous τ_w levels as a gas bubble and a liquid slug pass in the probe vicinity. The recording of the instantaneous τ_w value is of the form which is characteristic of intermittency. It is likely that the $\sqrt{(\overline{\tau_w'^2}/\overline{\tau_w})}$ increase in a slug regime is primarily due to the predominant role of large-scale low-frequency fluctuations assigned to the motion of large gas bubble and slugs relative to liquid.

3.3 *Void fraction profiles*

Profiles of the local void fraction for various U_1 and β values are shown in figure 14 (figures 14–18 illustrate regime B). The distribution of void fractions corresponding to various flow regimes are of different form. In a bubble regime there are sharp maxima near the tube walls, the central part of the profile is flat. In a fully developed slug regime the profile of the local void fraction is of the parabolic shape. It is interesting to note that the dependence between the ratio of the maximum value near wall α_m to the α_a value at the tube center and the liquid velocity is non-monotonous; the highest value of α_m/α_a is attained at $U_1 = 1$ m/s. A similar picture was also observed in the experiments performed by Serizawa (1975). The comparison of the

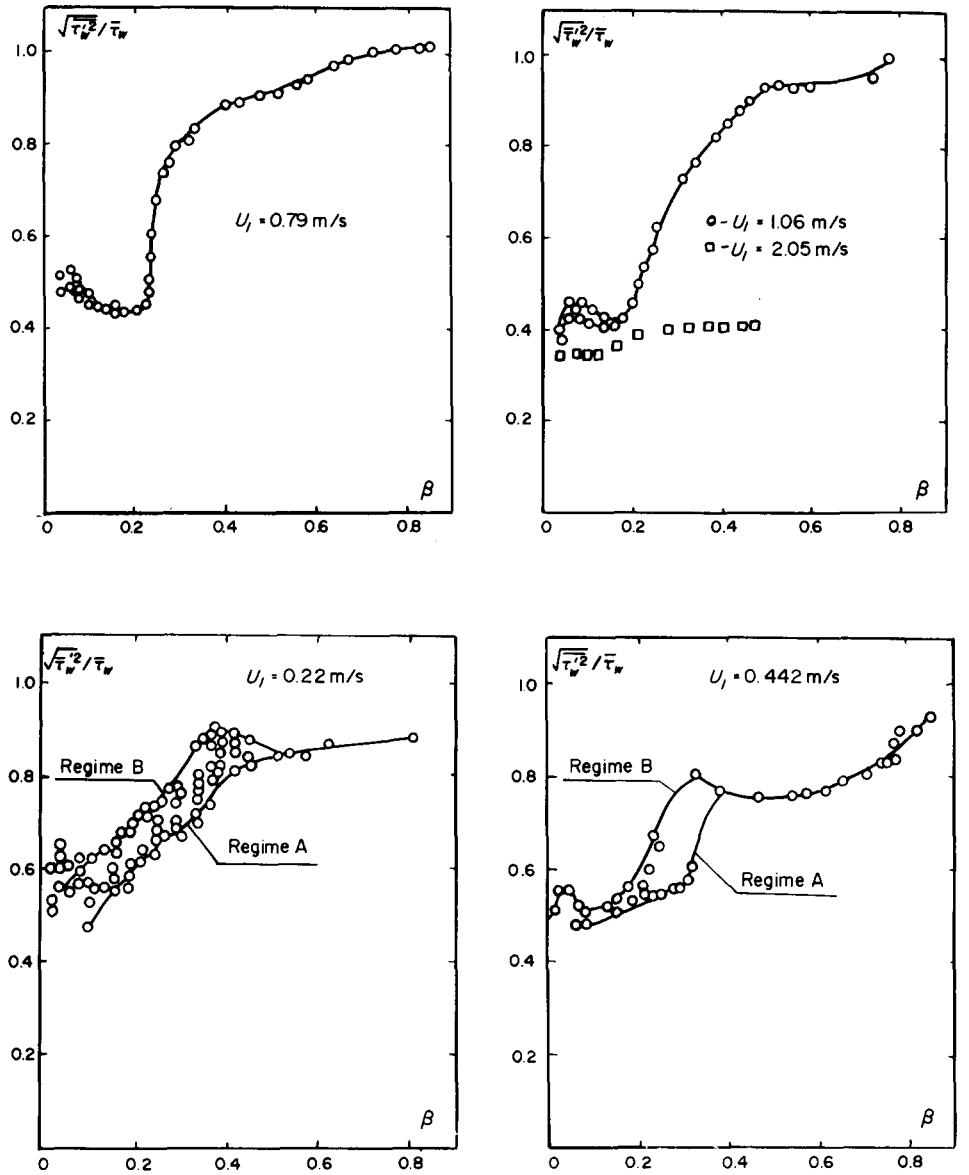

Figure 13. Intensity of wall shear stress fluctuations vs β

measured void fraction profiles with the distribution of wall shear stress (figures 11 and 12) shows that the void fraction peaks (near wall) lead to the significant wall shear stress increase. However, the α_m/α_a ratio is not the parameter unambiguously determining the above increase, since with increasing the liquid velocity at a constant β the τ_w/τ_{w_o} value monotonously decreases. Figure 15(a) represents the void fraction profiles at $U_l = 0.58$ m/s. It can be seen that at $\beta = 0.164$ the profile is of the specific shape with three peaks: two peaks are near the walls and one is at the tube center. This profile can be regarded as a combination of the profiles corresponding to the developed bubble and slug regimes. These profiles in the $\tau_w/\tau_{w_o}(\beta)$ plot correspond to the descending curve section which represents the bubble-to-slug flow transition. As shown above, this flow region is unsteady and its $\tau_w/\tau_{w_o}(\beta)$ ratio is of hysteresis type. At constant U_l and β the void fraction profiles can also be slightly different, namely they can have three peaks as in figure 8, and a point of contrary flexure (figure 14).

Figure 15(b) represents void fraction profiles at close β values but different liquid velocities U_l. At constant β with increasing the liquid velocity, the profile is reconstructed from that with

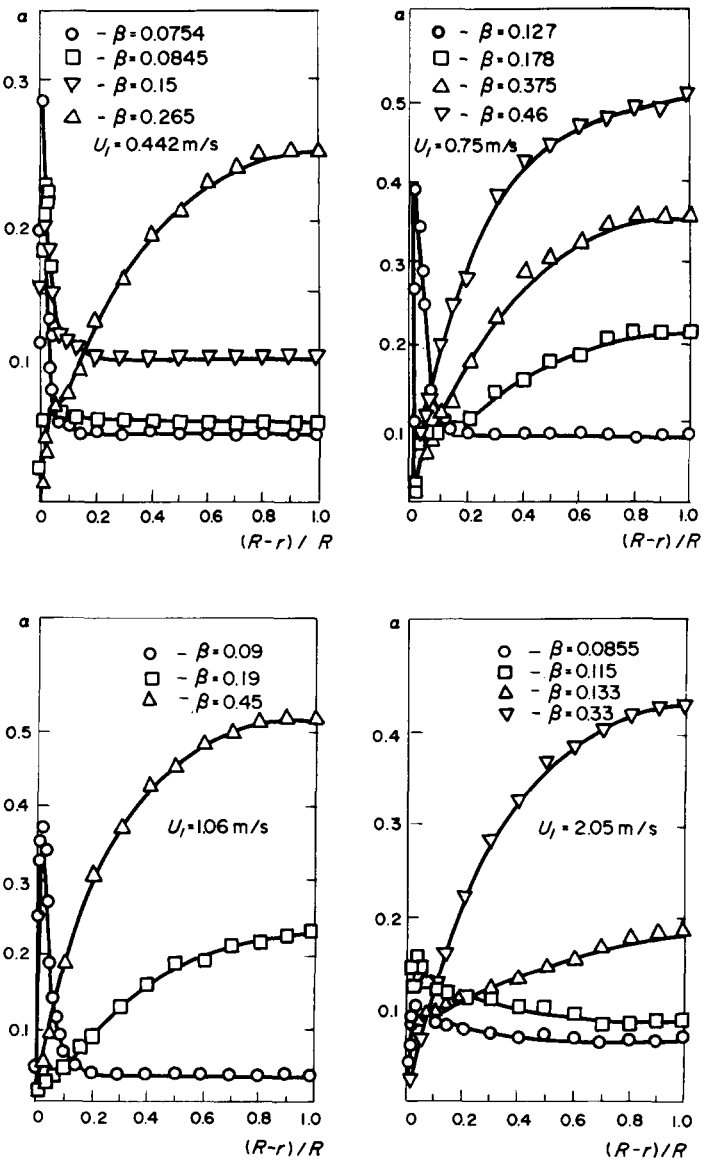

Figure 14. Profiles of local void fraction.

a peak near wall to the profile with a peak on the tube axis. It is likely that this is due to the increasing the mean velocity. These fluctuations prevent the bubble rushing to wall, from taking a steady position near it and smear them overall the tube cross section. At $U_1 = 2.05$ m/s (figure 15 b) even in a bubble regime the peaks near wall are slightly distinct, though still retained. It is evident that with increasing the liquid velocity, these peaks tend to decrease, and it it natural to suppose that at higher U_1 the peaks of α should completely vanish, as shown, e.g. by Herringe & Davis (1976). However due to the limitations of our experimental set-up we have not elucidated it.

3.4 *Liquid velocity profiles*

The significantly nonuniform distribution of gas concentrations across the channel section, particularly at low liquid velocities, changes the liquid velocity profile as compared to its shape in a pure liquid flow.

Liquid velocity profiles in a two-phase flow for various U_1 and β values are shown in figure 16. It can be seen that their shape considerably depends on the flow regime. In a bubble regime

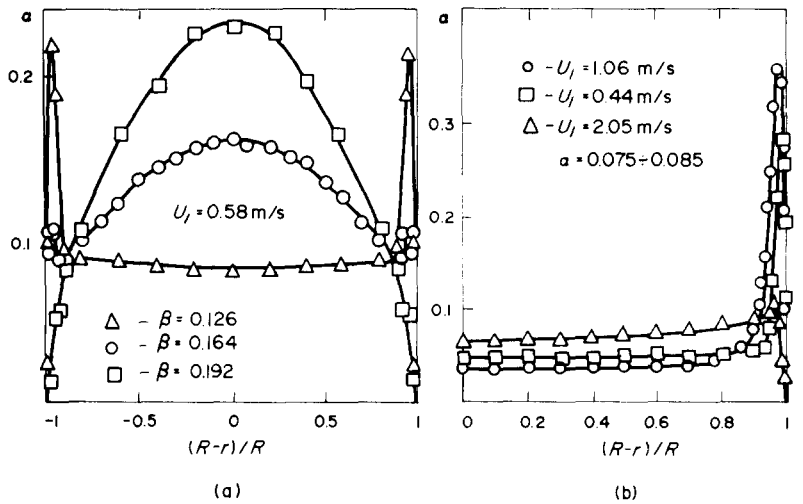

Figure 15. Profiles of local void fraction.

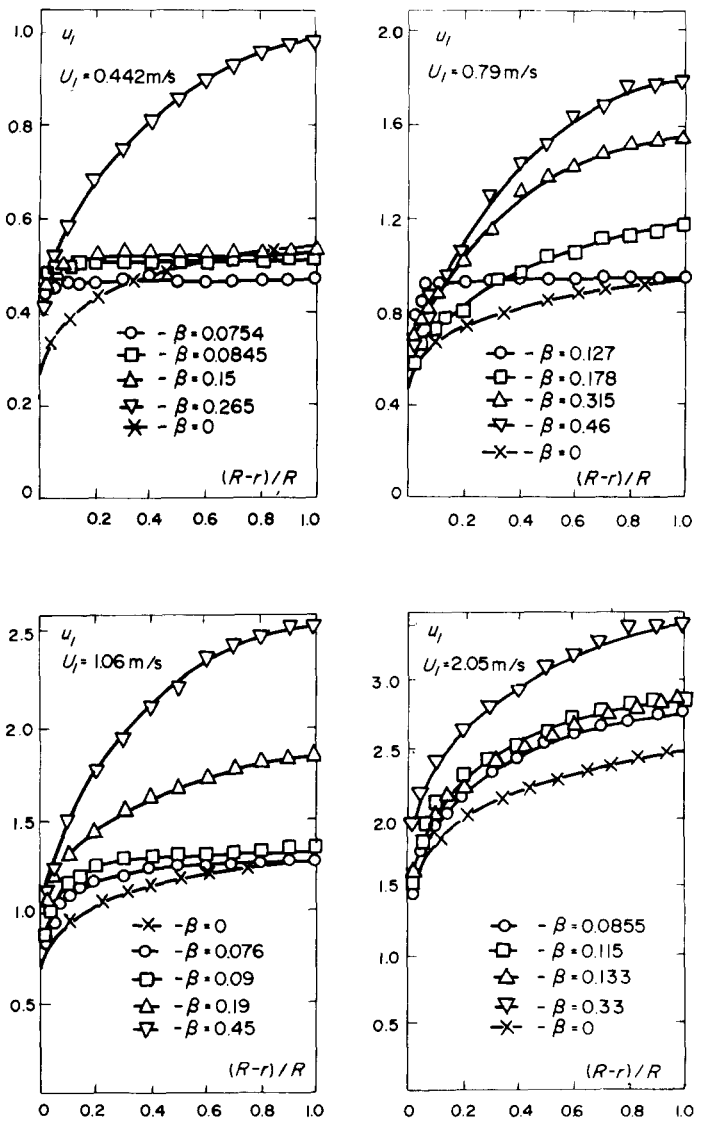

Figure 16. Liquid velocity profiles in two-phase flow.

the profiles are more flat and at low liquid velocities they are almost uniform. At the same time the profiles which correspond to a slug flow regime are more extended and their shape is parabolic. The gas phase in a flow leads to the increased liquid velocity as compared to a single-phase flow with the same liquid flow rate. The deformation of velocity profile is more clearly seen in figure 17, where the velocity profiles are given in the dimensionless form (the local velocity is divided by the velocity at the tube center). As a rule, more flatter are the profiles in the regimes having a peak of the local void fraction near wall. With the transition to a slug regime the profiles become less flatter than in a single-phase flow, and in several cases they can accidentally coincide (figure 17, $\beta = 0.19$). At $U_l = 2.05$ m/s velocity profiles at all void fractions are fairly close to that of a single-phase flow. In this case the flow behaviour can be considered as homogeneous, as $\alpha(r)$ distribution is nearly uniform.

Figure 18 represents the wall regions of velocity profiles. At $U_l = 0.44$ m/s in a bubble regime the velocity is constant even at a distance of about 1.5 mm from wall, which approximately equals to the gas bubble radius.

The results of turbulence index measurements for the liquid velocity fluctuations are given in figure 19. The intensity of velocity fluctuations in a two-phase flow is higher than in a single-phase one. In a bubble flow regime the increase of turbulence index near wall is insignificant and of the same order in magnitude as that in the intensity of wall shear stress

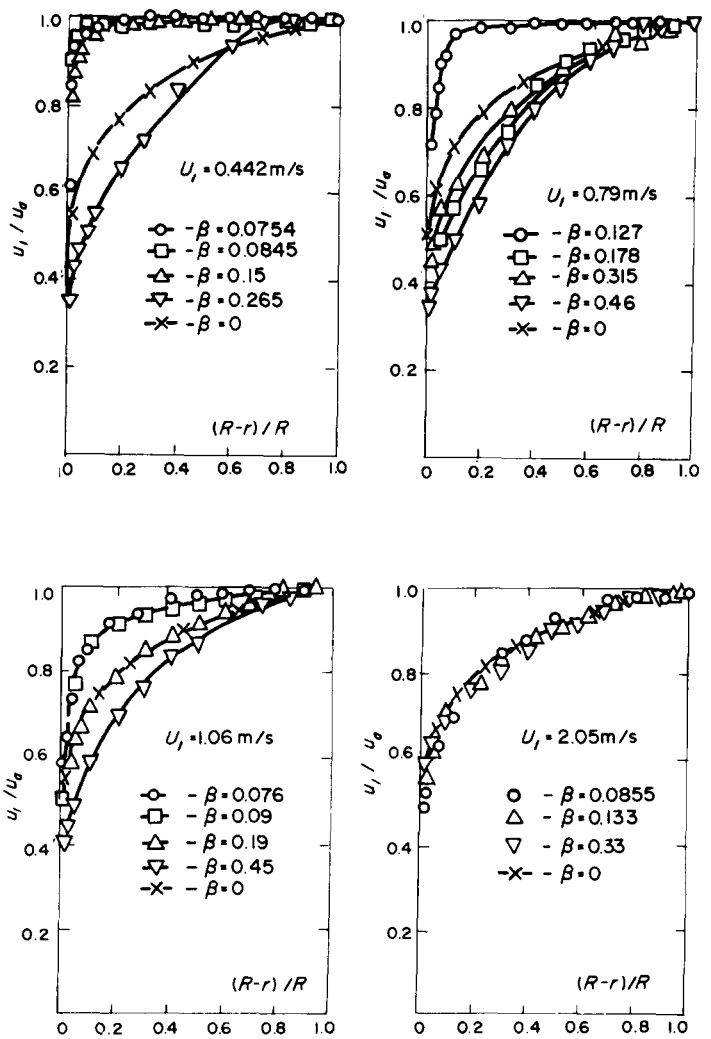

Figure 17. Profiles of reduced liquid velocity in two-phase flow.

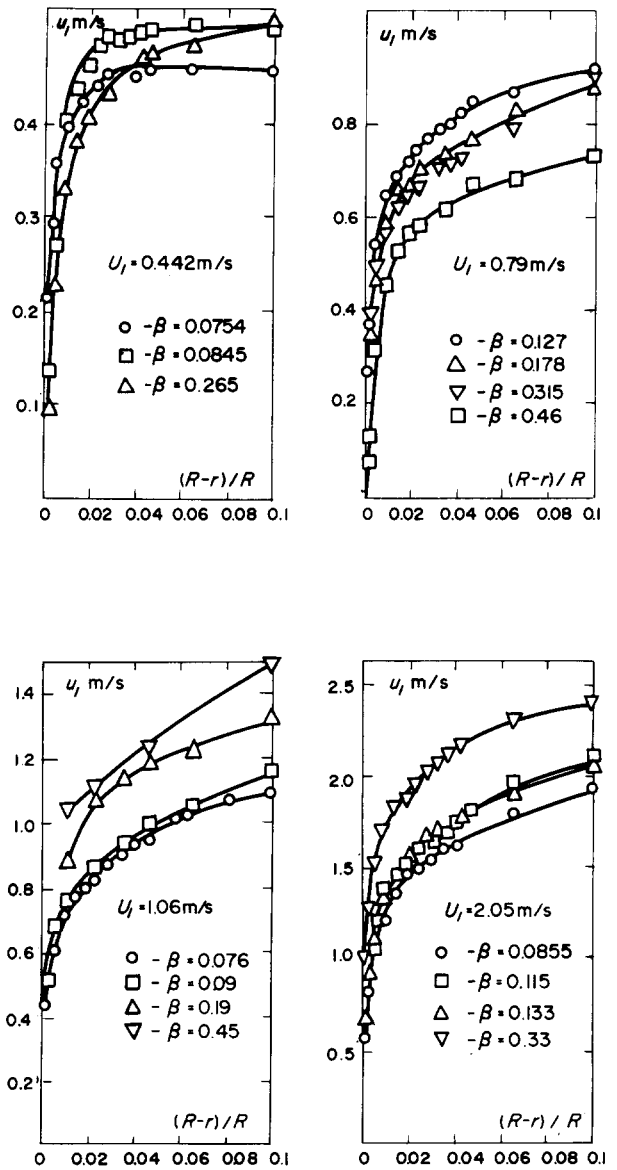

Figure 18. Profiles of liquid velocity in wall vicinity in two-phase flow.

fluctuations (figure 13). The most significant difference is observed at the central part of the tube. In a two-phase flow $\sqrt{(\overline{u_l'^2}/u_l)}$ at $(R-r)/R > 0.2$ remains practically constant, while in a single-phase flow this value monotonously decreases towards the axis. A very sharp increase in the turbulence index is observed in a slug regime at small liquid velocities. In this case the qualitative behaviour of turbulence index is the same as in a single-phase flow, through the numerical values are much higher. With increasing the liquid velocity for constant β the turbulence index in a slug regime decreases.

4. CONCLUSION

The application of an electrochemical method of measurement in a two-phase flow provides fairly complete information on the mean and fluctuational flow characteristics. Using the developed technique, we have performed a complex study of local void fractions and liquid velocity and completed it by the studies of wall shear stress and fluctuational flow characteristics. Using the developed technique, we have performed a complex study of local void

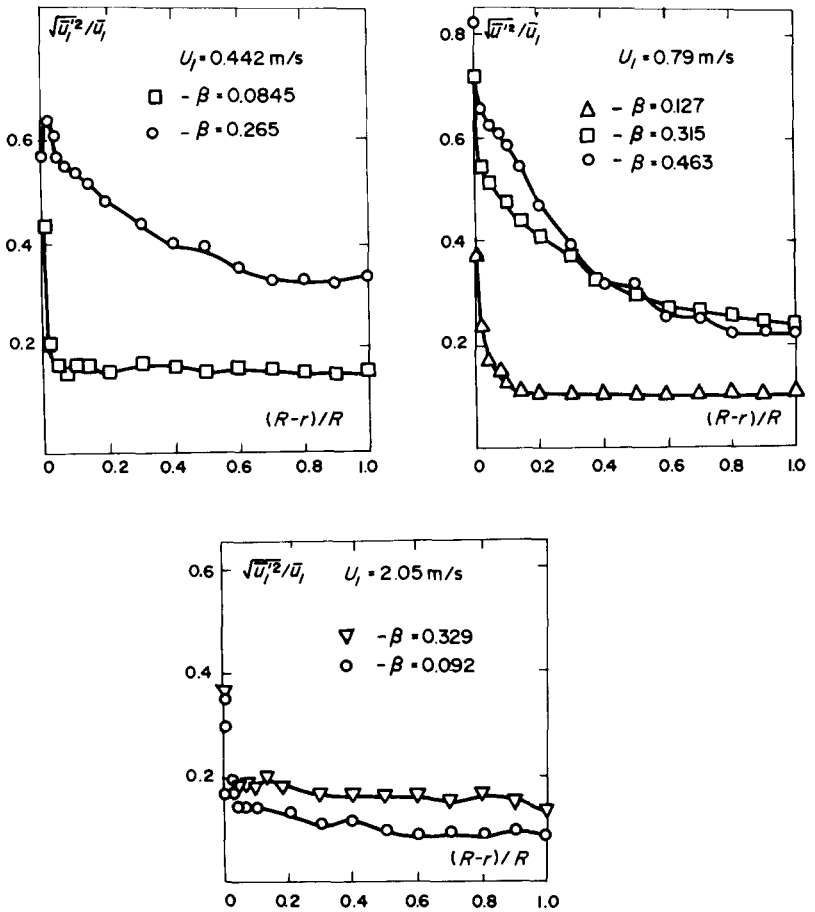

Figure 19. Profiles of intensity of liquid velocity fluctuations in two-phase flow.

fractions and liquid velocity and completed it by the studies of wall shear stress and fluctuational flow characteristics.

These studies show that the flow in a bubble regime at $U_l \leq 1$ m/s is of the hysteresis type and the existence of two stable bubble regimes is possible. This effect vanishes either with the U_l increase or with the increased void fraction and the transition to a slug regime.

Flow regimes with a distinct sharp peak of the void fraction in the wall vicinity are characterized by high values of wall shear stress, which are by 3–7 times higher than those calculated by standard (e.g. the Lockhart–Martinelli type) methods for two-phase flows.

The introduction of a gas phase into liquid in a bubble regime leads to the significant change in the mean flow characteristics and to a fairly slight increase in the intensity of turbulent velocity and wall shear stress fluctuations. At the same time in a slug regime the disturbing action of a gas phase considerably deforms both the mean and the fluctuational flow structures.

NOMENCLATURE

A, B calibration coefficients in formulae
A_1 coefficient in formula (6)
C_o concentration of active ions in solution
D diffusion coefficient
d characteristic size of velocity probe
F Faraday number
Fr Froude number
H frequency response function

h transverse size of wall shear stress probe
K mass transfer coefficient
L longitudinal size of wall shear stress probe
R tube radius
r coordinate of velocity probe measured from tube axis
Re Reynolds number
S probe surface area
u_l longitudinal velocity; local liquid velocity in two-phase flow
u_a velocity at tube center
U_g gas flow rate
U_l liquid flow rate
y coordinate measured from tube wall
β volumetric gas flow rate ratio
μ dynamic viscosity
ν kinematic viscosity
τ_w wall shear stress in two-phase flow
τ_{w_o} wall shear stress in single-phase flow
α local void fraction
α_a α value on tube axis
ω angular frequency
ω_* dimensionless frequency
ω_q critical frequency
— mean value
′ fluctuational value
m maximum value

REFERENCES

ARMAND, A. A. 1946 Pressure drop in a two-phase flow in horizontal pipes. *Izv. VTI* **I**, 16–23.

ARMAND, A. A. & NEVSTRYEVA, E. I. 1950 Investigation of mechanism of two-phase mixture transport in a vertical tube. *Izv. VTI* **2**, 1–8.

AOKI, S. & INOUE, S. 1965 Fundamental studies on pressure drop in an air-water two-phase flow in vertical pipes. Preprint of 2nd Japan. *Heat Transfer Symp.*, p. 137.

BOGOLYUBOV, YU. E., GESHEV, P. I., NAKORYAKOV, V. E. & OGORODNIKOV, I. A. 1972 Theory of electrodiffusion method of measurements of spectral characteristics in turbulent flows. *Zh. Prikl. Mekh. Tekh. Fiz.* **4**, 112–121.

BOGOLYUBOV, YU. E. & SMIRNOVA, L. P. 1977 Mass transfer near a stagnation point in a pulsating flow. *Izv. Sib. Otd. Akad. Nauk SSSR, Ser. Tekh. Nauk*, **2**, 34–39.

DAVIS, M. R. 1974 The determination of wall friction for vertical and horizontal two-phase bubbly flows. *Trans. ASME, J. Fluid Engng* **2**, 173–179.

DELHAYE, J. M. 1968 Anémométrie à fil chaud dans les écoulements diphasiques. Mesure du taux de présence du gas. *C.R. Acad. Sc.* **A266**, 370–373.

GALAUP, G. P. 1975 Contribution à l'étude des méthodes de mesure en écoulement diphasique. These, l'Université scientifique et médicale de Grenoble.

GOVIER, G. W., RADFORD, B. A. & DUNN, J. S. C. 1957 The upwards vertical flow of air–water mixtures—I. Effect of air- and water rates on flow pattern, holdup and pressure drop. *Can. J. Chem. Engng* **35**, 58–70.

HERRING, E. A. & DAVIS, M. R. 1976 Structural development of gas–liquid mixture flows. *J. Fluid Mech.* **73**, 97–123.

KAZIN, I. V. 1964 Radial distribution of vapour in upward turbulent steam–water flow. *Teploenergetika* **1**, 40–43.

KUTATELADZE, S. S., BURDUKOV, A. P., NAKORYAKOV, V. E. & KUZMIN, V. A. 1968 Application of electrochemical friction measurement method in hydrodynamics of two-phase media. In *Heat and Mass Transfer*, Vol. 2, pp. 367–375. Nauka i Tekhnika, Minsk.

KUTATELADZE, S. S. (Ed.) 1973 *Investigation of Turbulent Flows in Two-Phase Media.* Inst. Teplofiziki, Novosibirsk.

KOPALINSKY, E. M. & BRYANT, R. A. A. 1976 Friction coefficients for bubbly two-phase flow in horizontal pipes. *AIChE J.* **22**, 82–86.

LAUFER, J. 1954 The structure of turbulence in fully developed pipe flow. NACA Rep. 1174.

LOCKHART, P. W. & MARTINELLI, R. C. 1949 Proposed correlation of data for isothermal two-phase, two-component flow in pipes. *Chem. Engng Prog.* **45**, 39–48.

MAMAEV, V. A., ODISHARIYA, G. E., SEMENOV, N. I. & TOCHIGIN, A. A. 1969 *Hydrodynamics of Gas–Liquid Mixtures in Pipes.* Nedra, Moskva.

MISUSHINA, T. 1971 The electrochemical method in transport phenomena. In *Advances in Heat Transfer*, Vol. 7 (Edited by HARNETT, J. P. and IRVINE, T. F.), pp. 87–161. Academic Press, New York.

MITCHEL, J. & HANRATTY, T. J. 1966 A study of turbulence at a wall using an electrochemical wall shear stress meter. *J. Fluid Mech.* **26**, 199–221.

NEAL, L. G. & BANKOFF, S. G. 1963 A high-resolution resistivity probe for determination of local void properties in gas–liquid flow. *AIChE J.* **9**, 490–494.

REISS, L. P. & HANRATTY, T. J. 1963 An experimental study of the unsteady nature of the viscous sublayer. *AIChE J.* **9**, 154–160.

SERIZAWA, A., KATAOKA, I. & MICHIYOSHI, I. 1975 Turbulence structure of air-water bubbly flow—II. Local properties. *Int. J. Multiphase Flow* **2**, 235–246.

VALUKINA, N. V., KOZMENKO, V. K. & KASHINSKY, O. N. 1979 Characteristics of monodisperse gas–liquid flow in a vertical pipe. *J. Engng Phys.* **36**, 695–699.